PCCP

PAPER

View Article Online
View Journal | View Issue

Cite this: *Phys. Chem. Chem. Phys.*, 2023, **25**, 33056

Metal-insulator transition and resistive switching in Y-doped CeO_2 ceramics

Fawaz Almutairi, [ab] Meshari Alotaibi [c] and Anthony R. West [b]

Received 26th July 2023,
Accepted 26th November 2023

DOI: 10.1039/d3cp03562j

rsc.li/pccp

Y-doped ceria, $Y_{0.16}Ce_{0.84}O_{1.92}$, is an oxide ion conductor that shows n-type conductivity under a small applied voltage. With increasing voltage, resistive switching by 2–3 orders of magnitude occurs that is reversible with some hysteresis and is enhanced in atmospheres of reduced pO_2. The switching is a bulk effect, is not associated with Schottky barriers or with a crystallographic transition, occurs rapidly after a premonitory onset period depending on conditions and shows characteristics of a Mott transition. This is the third known example of low field-induced resistive switching in a bulk ceramic and represents an emergent phenomenon in materials that are taken outside their zone of thermodynamic stability.

Introduction

Resistive switching phenomena in bulk materials are usually associated with phase transitions and are often described as metal-insulator transitions.[1] A new type of resistive switching (RS) in bulk materials has been reported in two recent examples, Ca-doped $BiFeO_3$ (BCF)[2] and Y-doped HfO_2, yttria-stabilised hafnia (YSH),[3] in which switching occurs in response to the application of a small voltage but does not involve any phase transition. It appears to be a different phenomenon to the voltage-induced switching observed in widely-studied memristive effects that is limited to thin films of nanometre dimensions and is associated with the formation and rupture of conducting filaments.[4–12]

Both BCF and YSH show different levels of mixed oxide-ion and p-type conductivity associated with the presence of oxygen vacancies. The oxygen vacancies charge-compensate the acceptor (lower valence) dopants, *i.e.* Ca^{2+} in place of Bi^{3+} and Y^{3+} in place of Hf^{4+}. The p-type conductivity in YSH is attributed to hole creation:

$$V_O^{\bullet\bullet} + \frac{1}{2}O_2 \rightarrow O_O^x + 2h \quad (1)$$

The holes appear to be located on lattice oxide ions, $O_O^{\bullet}$ whose number increases by a redox process involving reaction of lattice oxygen, O_O^x with oxygen vacancies, $V_O^{\bullet\bullet}$ and atmospheric oxygen, O_2:

$$V_O^{\bullet\bullet} + O_o^x + \frac{1}{2}O_2 \rightarrow 2O_O^{\bullet} \quad (2)$$

The p-type conductivity can also be introduced, or increased, on application of a small dc bias in the range 0.5–40 V, depending on the material and temperature.[3,13,14] With increasing bias, both BCF and YSH showed a gradual increase in p-type conductivity that concluded with a rapid switch, by 2–3 orders of magnitude, to a high conductivity 'ON' state. On removing the bias, the conductivity switched back to the original 'OFF' state with some hysteresis.[3,13] With increasing bias and before the OFF–ON switching occurred, the electronic conduction mechanism in YSH became n-type which led to the suggestion that a pn transition may be involved as well as oxygen exchange between samples and atmosphere.[3] Undoped $BiFeO_3$ does not show the same RS behaviour and in general, other stoichiometric materials, such as $BaTiO_3$, are not sensitive to a small dc bias. When they are acceptor-doped, however, their electronic conductivity becomes p-type and dependent on voltage and pO_2.[13–16]

The purpose of the present study was to determine whether low field-induced RS occurs in materials that are mixed conductors but n-type, rather than p-type in their electronic component, to gain further understanding of the RS process and the range of material types that may show this effect. This type of RS is an emergent phenomenon in which materials are taken outside their zone of thermodynamic stability but retain sufficient kinetic stability that they do not decompose with applied voltages that are above their decomposition potential.[27]

Pure and doped ceria (CeO_2) materials are well-known mixed oxide ion and n-type conductors.[17,18] They have higher ionic conductivity than YSZ at intermediate temperatures (400–700 °C), good thermodynamic stability[19] and have been studied intensively due to application possibilities as electrodes and electrolytes in solid oxide fuel cells (SOFC) and catalysts.[20–23] CeO_2 has the cubic fluorite structure, its defect structure has been well-studied,[24] it is stable over the whole temperature

[a] *Department of Physics, College of Science, Al Imam Mohammad Ibn Saud Islamic University (IMSIU), Riyadh, Saudi Arabia*
[b] *University of Sheffield, Dept of Materials Science & Engineering, Mappin St, Sheffield S1 3JD, UK*
[c] *Department of Chemistry, Faculty of Science, Taif University, Taif, Saudi Arabia*

range up to its melting point[17] and is very tolerant to doping by lower valence elements such as Y and rare earths, generating oxygen vacancies by mechanisms such as:

$$Y_2O_3 \rightarrow 2Y'_{Ce} + V_O^{\bullet\bullet} + 3O_o^x \quad (3)$$

Their mixed conductivity is due to reduction of Ce^{4+} to Ce^{3+} at high temperature (>800 °C) and/or in reducing atmospheres[18,23] in which lattice oxide ions are released according to:

$$O_O^x \rightarrow \frac{1}{2}O_2 + V_O^{\bullet\bullet} + 2e' \quad (4)$$

It was anticipated that electronic conductivity may also be induced in yttria-doped ceria at low temperatures by application of a small dc bias giving either single or double ionisation of oxide ions and either hole or electron conductivity, eqn (2) and (4), respectively, similar to that observed in the oxide ion conductors YSZ and YSH.[25,26]

Experimental

Samples of yttria-doped ceria (YDC), $Ce_{0.84}Y_{0.16}O_{1.92}$ were prepared by solid state reaction of CeO_2 (99% Sigma-Aldrich) and Y_2O_3 (99.99% Alfa Aesar) at 1400 °C for 12 h. Reagents were dried overnight at 900 °C before weighing, manually mixed in a conventional mortar and pestle with acetone, dried and reacted in an alumina crucible. The reacted powders were re-ground and pressed into pellets, 10 mm diameter and thickness of 1.5–3 mm, using a uniaxial press and sintered at around 1500 °C.

The sintered pellets were crushed and analysed using X-ray powder diffraction for phase identification a using Bruker D2 phaser with Cu Kα radiation (λ = 1.5418 Å). The data were collected over the range $20^\circ < 2\theta < 90^\circ$.

Ceramic electrical properties were measured and analysed using impedance spectroscopy. For impedance measurements, Au paste was attached to opposite sides of sintered pellets and dried at 850 °C for 2 hours. A pellet with attached electrodes was placed between Pt leads in an in-house measuring jig and placed in a tube furnace. Impedance measurements were performed as a function of different variables: (i) temperature, (ii) oxygen partial pressure, pO_2, (iii) dc bias and (iv) combination of dc bias and pO_2. Three impedance analysers were used which were Modulab XM Solartron with a frequency range 0.1 Hz-1000 kHz, Solartron SI 1260 with a frequency range 0.1 Hz-1000 kHz and Agilent 4294A with a frequency range 0.04–1000 kHz.

The collected data were corrected for jig impedance characteristics in which closed circuit measurements were performed to eliminate the lead inductance and resistance; open circuit measurements were performed to eliminate the blank capacitance of the jig. The data were corrected for the overall sample geometry in which the specific values of sample resistance, R and capacitance, C, *i.e.* resistivity, ρ and permittivity, ε are given by eqn (5) and (6), respectively:

$$\rho = RA/d \quad (5)$$

$$\varepsilon = Cd/A \quad (6)$$

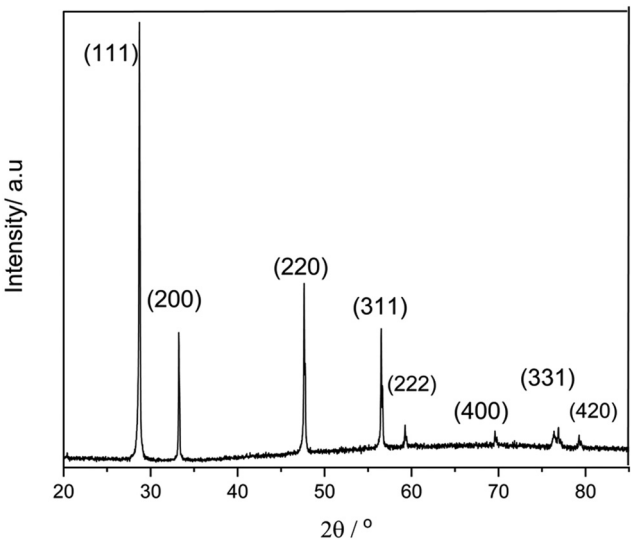

Fig. 1 XRD pattern of $Ce_{0.84}Y_{0.16}O_{2.92}$ showing a single phase, cubic fluorite structure.

where A is the cross section area of the pellet and d its thickness. Therefore, resistivity and permittivity are quoted in units of Ω cm and F cm^{-1}, respectively.

Results

Fig. 1 shows the XRD pattern of $Ce_{0.84}Y_{0.16}O_{1.92}$ which confirms that the sample was single phase. Data were indexed on a cubic unit cell, consistent with the data reported in the literature.[19,22]

A selection of impedance data, Fig. 2, over the range 245–506 °C show the presence of three components which were attributed, from their capacitance values of approximately 15 pF cm^{-1}, 3 nF cm^{-1} and 400 μF cm^{-1}, to sample bulk, grain boundary and sample-electrode interfaces, respectively. The low frequency impedance response is typical of oxide ion conduction that is in series with an element containing a double layer capacitance, C_{dl} in parallel with a charge transfer resistance, RCT, inset (a).

Arrhenius plots of bulk, grain boundary and total conductivities are shown in Fig. 3. Activation energies in the range 0.83–0.94 eV are consistent with literature data on oxide ion conductivity of doped ceria. The grain boundary activation energy, 0.94(2) eV, is slightly higher than the bulk value, 0.83(1) eV which may reflect a difference in either local structure or composition of the grain boundary.

The effect of pO_2 on impedance data at 417 and 506 °C, Fig. 4, shows that the sample conductivity was independent of pO_2 and the sample was in the electrolytic domain of oxide-ion conductivity at these temperatures, consistent with that reported in.[19] Only the sample-electrode interface resistance was sensitive to pO_2, as shown by a dramatic decrease in conductivity Y' at low frequency in N_2, Fig. 4(b) and (d). This showed that the O_2/O^{2-} charge transfer resistance increased greatly at low pO_2 and was further evidence that the sample was an oxide ion conductor.

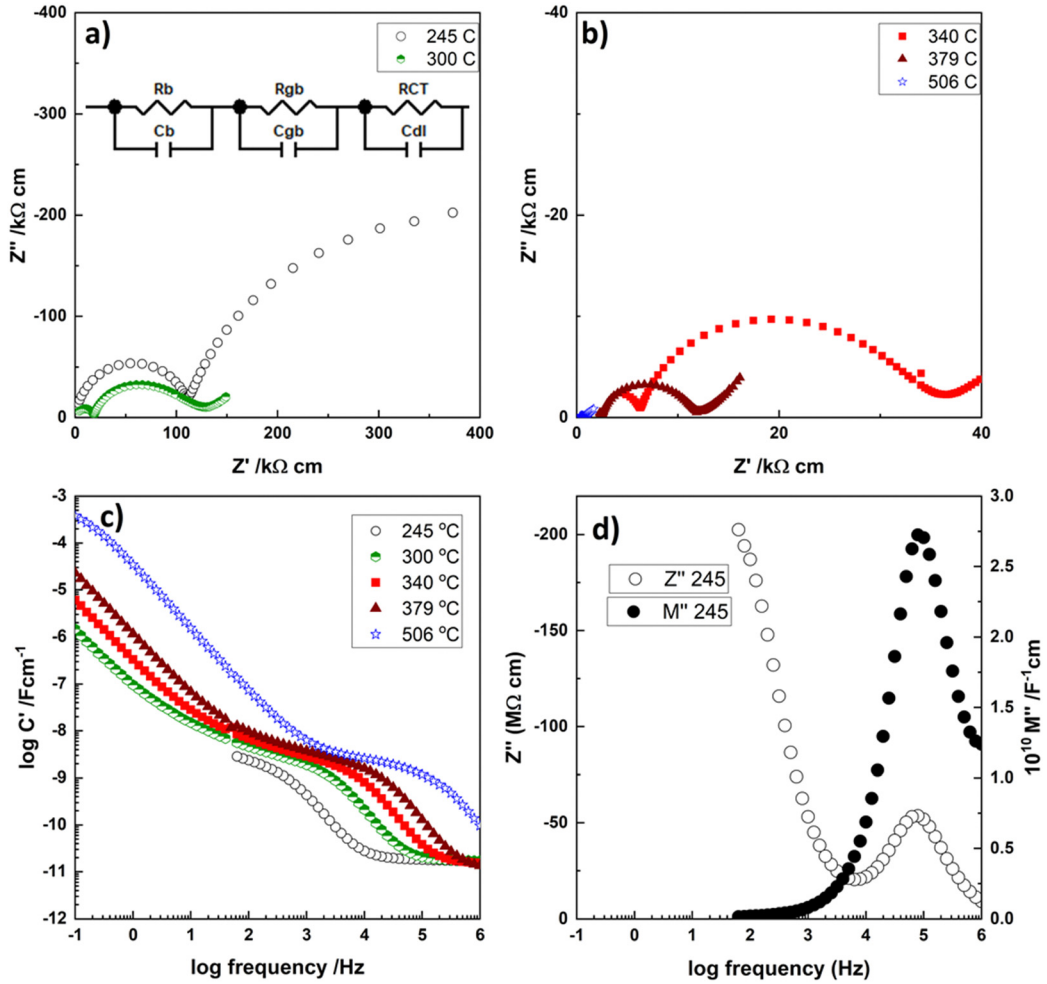

Fig. 2 Impedance complex plane plots, Z^* at (a) 245, 300 °C and (b) 340, 379 and 506 °C. The ideal equivalent circuit to represent the impedance data is shown as inset (a); for accurate data fitting, constant phase elements would be added to the ideal circuit. (c) C' spectroscopic plots at different temperatures; (d) Z''/M'' spectroscopic plots.

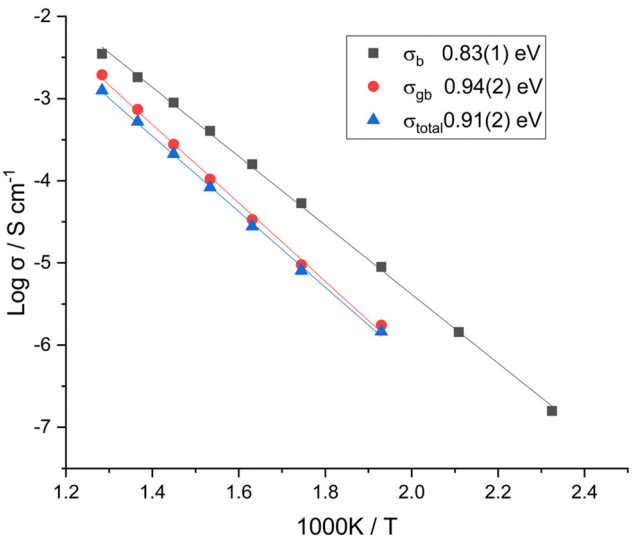

Fig. 3 Arrhenius plot of bulk, grain boundary and total conductivity of $Ce_{0.84}Y_{0.16}O_{2.92}$.

The effect of dc bias on the impedance response in different atmospheres at 353 °C is shown in Fig. 5. All three resistances, bulk, grain boundary and total, decrease with increasing voltage and the decreases are greater in N_2 than in O_2. These results indicate that electronic conductivity is induced by application of a small dc bias, similar to that observed in YSZ08.[25,27] The resulting conductivity is n-type because O_2 loss under bias at low pO_2, eqn (4) is accompanied by electron injection into the sample and presumably leads to the creation of Ce^{3+} ions which are the main electron carrier.

With increasing voltage at 366 °C in N_2, the total conductivity increased slightly until, at 105 V cm^{-1}, a sudden switch to a higher conductivity ON state occurred, Fig. 6. The conductivity increased abruptly by about two orders of magnitude (a); on decreasing the field, the ON state conductivity increased a little until, below 55 V cm^{-1}, it decreased abruptly to its original value. The measurements were done on three different samples with different dimensions and repeated up to 8 cycles to check data reproducibility. The data reported in Fig. 6a show that the ON–OFF switching behaviour was reproducible with no obvious change in the data after 8 cycles. The

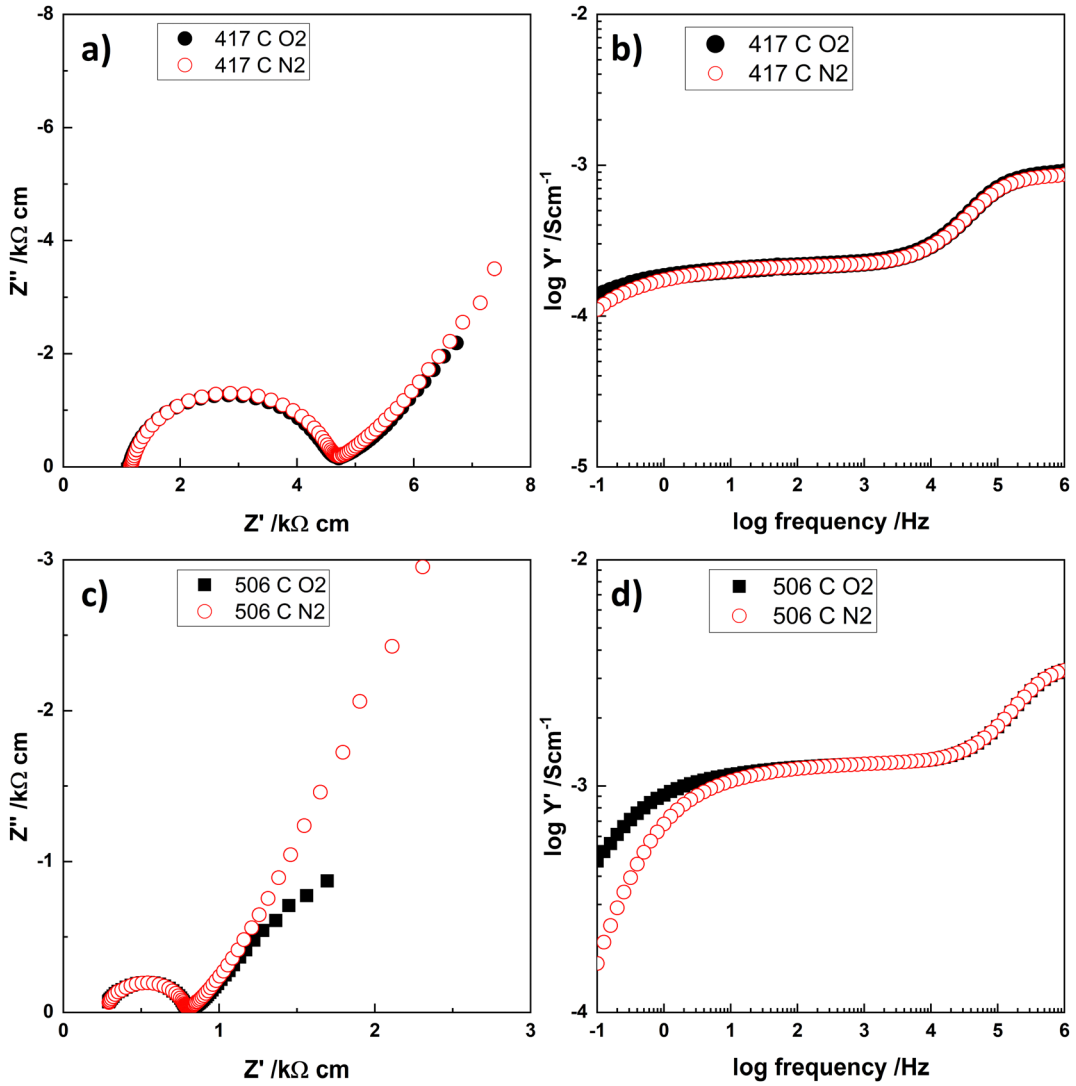

Fig. 4 (a) and (c) impedance complex plane plots, (b) and (d) *Y′* spectroscopic plots of $Ce_{0.84}Y_{0.16}O_{2.92}$ measured in O_2 and N_2 at different temperatures.

switching behaviour was independent of polarity of applied voltage (not shown) and the sample switched similarly in both directions.

A further indication of the effect of pO_2 on this RS behaviour is shown by the time dependence of the total conductivity in response to 119 and 155 V cm^{-1} at 366 °C in N_2 and air (b) and (c). At the lower voltage, 119 V cm^{-1} (b), the conductivity in air increased slightly but remained in the OFF state for 200 minutes, whereas in N_2 the sample showed premonitory increase in conductivity before a rapid switch to the ON state after 125 minutes. However, at the higher voltage, 155 V cm^{-1} (c), the sample showed similar premonitory increases in conductivity before rapid switching to the ON state in both air and N_2. The rapid increase in conductivity occurred earlier in N_2 and the ON state conductivity was highest in N_2. With both applied biases, on removal of the bias, the sample recovered its original conductivity rapidly after a similar time in both air and N_2.

Further investigation of the effect of pO_2 on the switching mechanism and conductivity in the ON state is shown in Fig. 7. The samples had been switched to the ON state at 620 °C by application of 20 V in atmospheres of either N_2 and O_2 and the conductivities shown were measured, with the voltage applied, on cooling in the same atmosphere; data recorded with 0 V are shown for comparison. In N_2, the sample maintained the ON state on cooling to 100 °C with a gradual decrease in both conductivity and activation energy, especially at lower temperatures. In O_2, the sample maintained the ON state over a more limited temperature range and gradually switched back to the OFF state below 250 °C. During cooling in the two atmospheres, the ON state conductivity was highest in N_2.

The impedance of samples before and after passing through the ON–OFF cycle showed no significant differences, Fig. 8, indicating that no obvious irreversible changes, such as degradation under applied voltage, occurred during the switching process.

Discussion

CeO_2 is a well-known MIT material for thin film devices which shows both bipolar and unipolar switching.[28–32] For example, a

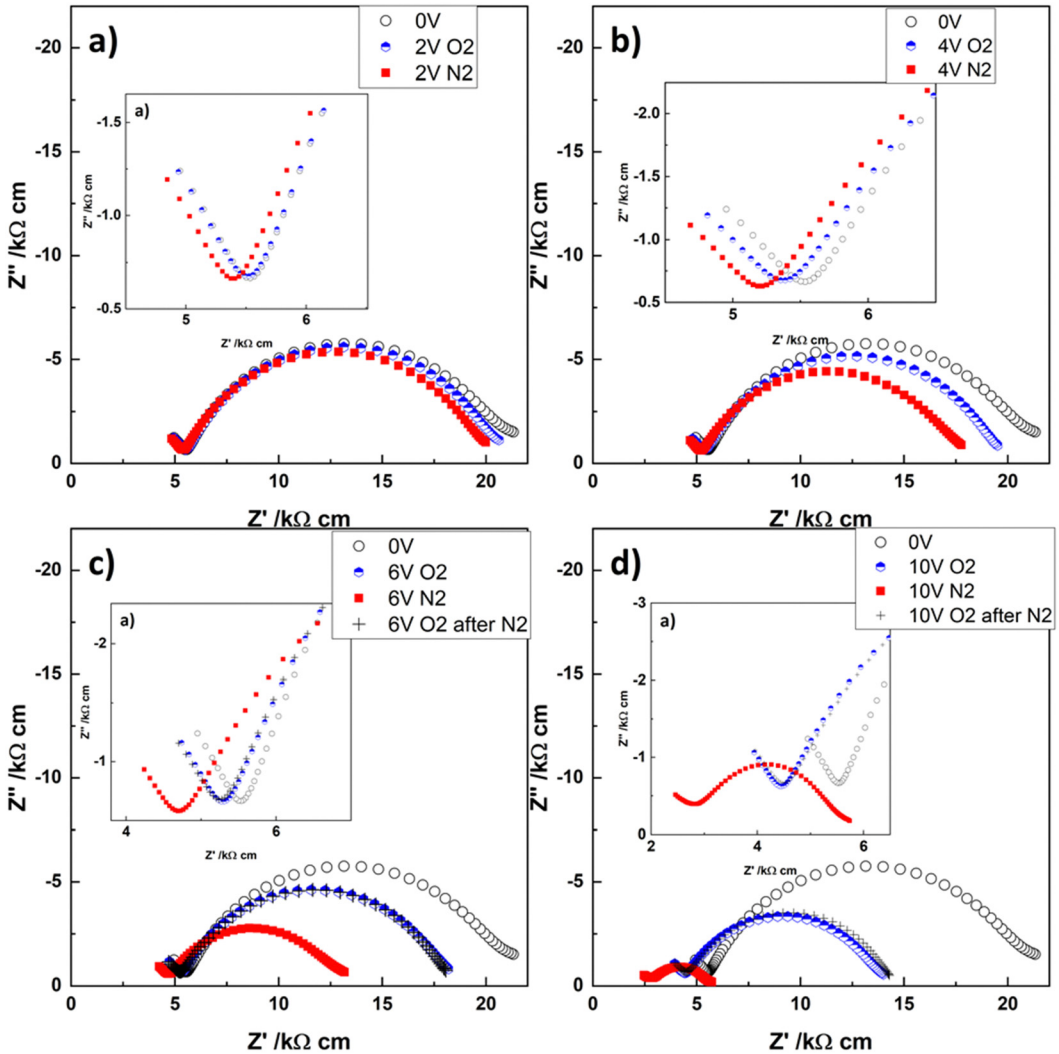

Fig. 5 Impedance complex plane plots of $Ce_{0.84}Y_{0.16}O_{2.92}$ measured in different atmospheres at 353 °C on application of (a) 2 V, (b) 4 V, (c) 6 V and (d) 10 V.

device made of 50 nm layer of CeO_2 with sequence of Ag–Ti–CeO_2–Pt showed stable repeatable bipolar and unipolar RS.[32] In both switching types, the device maintained the new resistance state until rest voltage was applied (*i.e.* the device has two stable states, ON and OFF state, in the absence of electrical field). In bipolar switching, the device switched to low resistance state at about +0.3 V and recovered its original state at about − 0.5 V. In many studies[28–32] such devices showed good endurance and retention in which the device can maintain the ON and OFF state up to 10^5 s.

The RS in yttria-doped ceria, YDC is clearly electronic in origin but also different from the unipolar and bipolar switching of thin film memristors that require re-application of a bias voltage to recover the original conductivity[4] while in the absence of the electrical field, YDC has only one stable state, OFF state (Fig. 6). It occurs over an entirely different length scale, 1 to 10 mm, to that involved in switching thin film memristors, 1 to 10 nm. The applied voltages used with memristors, typically 1–2 V, are at the lower end of those used with bulk ceramics, 1–40 V, but the average field gradients must differ by six orders of magnitude. A direct comparison of the fields used in the two sets of materials is difficult, however, because in the bulk ceramics, the field may be localised initially at resistive ceramic-electrode interfaces. It is difficult to compare these results with RS in a thin film device due to these differences and especially, since our work is on millimetre thick samples. Therefore, further work is required to check our results on nanoscale materials for possible device applications and to establish whether the RS in bulk ceramics and thin film memristors have a common origin. Our results are comparable to recently-reported RS in two types of bulk materials: perovskite-structured Ca-doped BF (BCF) and fluorite-structured YSH.

YDC is the third example, after Ca-doped BF and YSH, to show this kind of resistive switching in bulk ceramics. In response to application and removal of a small dc bias, all three cases show a premonitory period of increased conductivity followed by a rapid, reversible increase, with hysteresis, in the conductivity by a few orders of magnitude. There is a threshold set of conditions involving three inter-dependent parameters: voltage, temperature and atmosphere, for RS to occur.

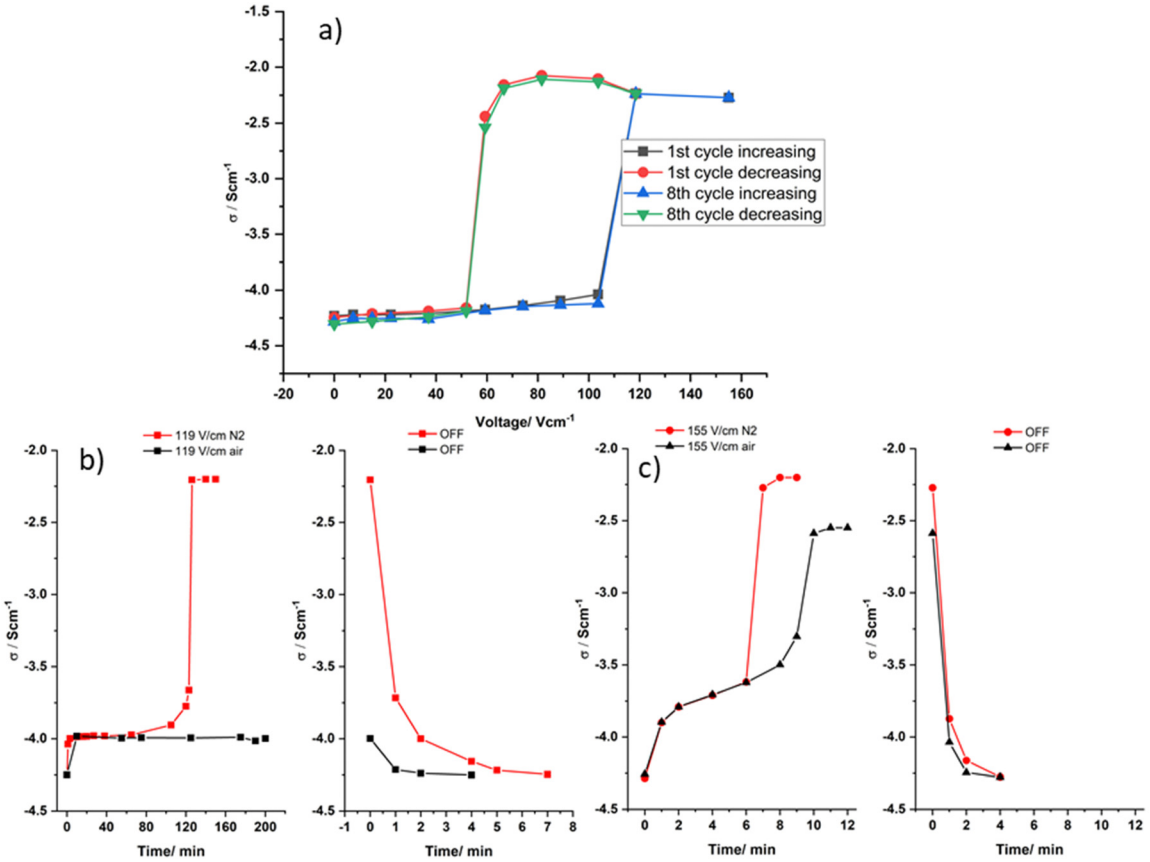

Fig. 6 The total conductivity of $Ce_{0.84}Y_{0.16}O_{2.92}$ at 366 °C (a) after reaching steady state *vs.* applied voltage in N_2, (b) and (c) against time on applying and removing 119 and 155 V cm^{-1} in air and N_2.

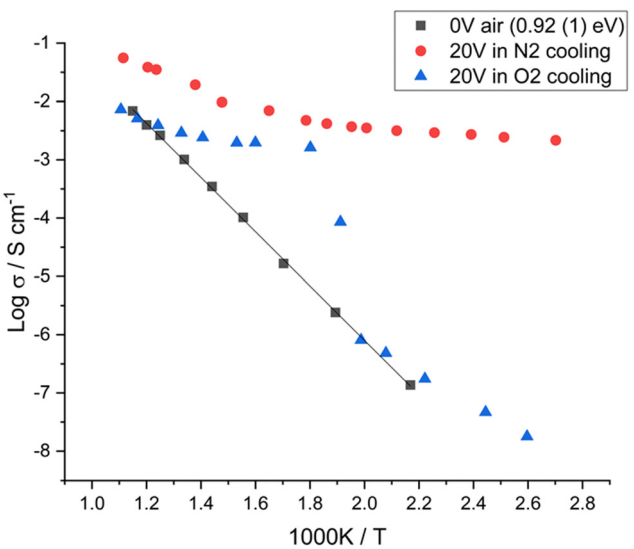

Fig. 7 Arrhenius plots of total conductivity in OFF state in air and on cooling with application of 20 V (158 V cm^{-1}) in N_2 and in O_2.

There is no evidence of any crystallographic phase transition and the switching is reversible, with hysteresis, without showing sample degradation. Thus, we have no direct evidence of crystallographic changes to form the ON state or whether, as proposed, Ce^{4+} ions are reduced to Ce^{3+}. However, since the ON state has almost zero activation energy for conduction, it is likely that a band model for conductivity is required, in which case, it may no longer appropriate to refer to the ionic 3+ and 4+ states of Ce.

RS occurs in both bulk and grain boundary components and is not associated with any Schottky barrier at the sample-electrode interfaces. All three materials are acceptor-doped and show different levels of mixed oxide-ion and electronic conductivity, depending on conditions. They have oxygen vacancies as the main charge compensation mechanism but differ in the nature of their electronic conductivities which is p-type in BCF, changes from p- to n-type with increasing voltage in YSH, but is n-type in YDC.

The RS mechanism in YSH was attributed to the possible breakdown of a p–i–n junction in which p- and n-type conductivities were created at opposite electrodes in response to application of the dc bias,[3] with the implication that one of the electronic components, presumably the n-type, dominated the ON state conductivity. The RS mechanism in BCF may initiate with hole injection at the anode to form a p-type surface layer that thickens and grows into the sample interior[2] since it showed no evidence of any n-type conductivity during or after the switching. Evidence for hole injection and growth of a

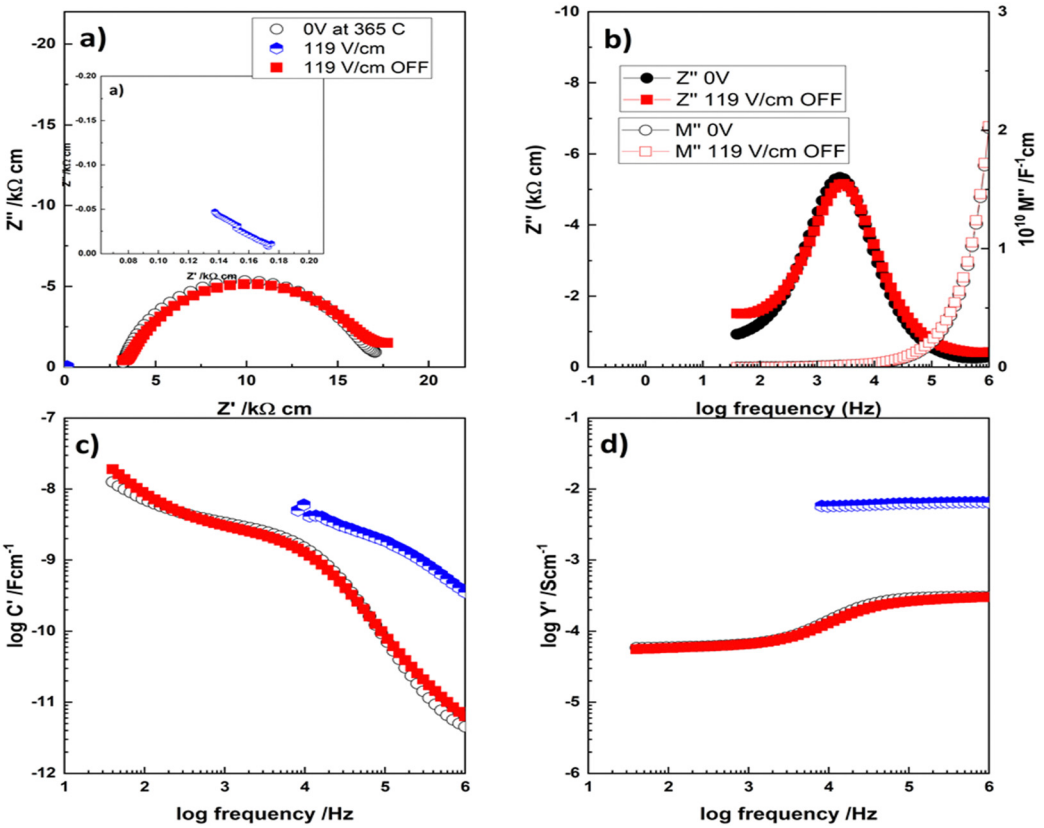

Fig. 8 The impedance response of $Ce_{0.84}Y_{0.16}O_{2.92}$, before application, during and after removal of 119 V cm^{-1}.

p-type region was obtained in related studies of Mg-doped $BaTiO_3$ in which electric modulus, M'' presentations of impedance data showed that the initial bulk impedance component was gradually replaced by a more conductive bulk component.[13] The total conductivity increased by several orders of magnitude under certain conditions but remained p-type and did not achieve resistive switching.

In contrast to YSH and BCF, YDC showed RS that was n-type in both the low field OFF state and high field ON state. The n-type conductivity is attributed primarily to loss of oxygen, especially in atmospheres of low pO_2 and is associated with electron injection at the negative electrode and probable reduction of Ce^{4+} to Ce^{3+} to give an n-type layer that thickens and grows towards the anode. It appears that the RS mechanism in YDC is similar to that in BCF, therefore, but different in carrier type and source of the electronic conductivity.

We conclude that several factors influence RS and that conductivity can be either p-type or n-type in the ON state, depending on the material. The ON state conductivity of YDC, Fig. 7 and BCF has very low activation energy indicating that the carrier concentration becomes constant and a band model for conduction is appropriate. This is in contrast to the OFF state for which the high activation energies indicate a model of carrier localisation and hopping conduction. Depending on experimental conditions, the RS in YDC, as for the other two cases, involves a sharp transition that follows a premonitory region of gradually increasing conductivity. All three cases appear to involve an increase in carrier concentration that may also be described as either a change from small-to-large polaron conduction or a Mott transition[1] both of which involve an increase in number, and delocalisation, of the charge carriers. Evidence for this may come from the premonitory period of increasing conductivity prior to switching, in which the conductivities are time-independent once a steady state is reached; the conductivity increase could be attributed to a gradual increase in polaron size and/or delocalisation of the charge carriers.

Oxygen exchange between sample and atmosphere appears to be an important parameter in all three RS cases and leads to major changes in carrier concentration. The time-dependence of switching that is frequently observed may depend on bulk diffusion of oxide ions within the host lattice and therefore, on the presence of oxygen vacancies and oxide ion conductivity although, of course, the RS process itself is electronic in origin.

Conclusions

Single phase $Ce_{0.84}Y_{0.16}O_{1.92}$ sintered in air is primarily an oxide-ion conductor. n-type electronic conductivity induced by applying a small dc bias is attributed to oxygen loss and liberation of electrons which reduce Ce^{4+} to Ce^{3+}. At higher bias, reversible resistive switching occurs leading to a high conductivity ON state with delocalised charge carriers. The switching has characteristics of a metal-insulator transition

but is not associated with a crystallographic phase transition. YDC is the third example to show low-field resistive switching in a bulk ceramic.

Low field-induced RS is an example of emergent phenomena in which the effect of an applied voltage that is above the theoretical decomposition potential of a material is to create a domain of thermodynamic metastability but kinetic stability. In this domain, the materials retain their essential crystal structure but may undergo voltage-induced reversible changes to bond character, defect structure or sample homogeneity without undergoing complete decomposition. Examples of such emergent phenomena are V-induced RS of bulk ceramics, memristive switching of thin films, flash sintering of ceramics and charging of Li, Na battery cathodes by a mechanism that combines a redox reaction and Li or Na de-intercalation.[26]

Conflicts of interest

The authors have no conflicts to disclose.

Acknowledgements

Fawaz Almutairi thanks Al Imam Mohammad Ibn Saud Islamic University for a studentship.

References

1 N. F. Mott, *Rev. Mod. Phys.*, 1968, **40**, 677.
2 N. Maso, H. Beltran, M. Prades, E. Cordoncillo and A. R. West, *Phys. Chem. Chem. Phys.*, 2014, **16**, 19408–19416.
3 M. Alotaibi, F. Almutairi and A. R. West, *J. Am. Ceram. Soc.*, 2022, **106**, 822–828.
4 J. S. Lee, S. Lee and T. W. Noh, *Appl. Phys. Rev.*, 2015, **2**, 031303.
5 D. Kumar, R. Aluguri, U. Chand and T. Y. Tseng, *Ceram. Int.*, 2017, **43**, S547–S556.
6 A. Sawa, *Mater. Today*, 2008, **11**, 28–36.
7 D. Panda and T.-Y. Tseng, *Ferroelectrics*, 2014, **471**, 23–64.
8 K. M. Kim, D. S. Jeong and C. S. Hwang, *Nanotechnology*, 2011, **22**, 254002.
9 B. J. Choi, S. Choi, K. M. Kim, Y. C. Shin, C. S. Hwang, S.-Y. Hwang, S.-S. Cho, S. Park and S.-K. Hong, *Appl. Phys. Lett.*, 2006, **89**, 012906.
10 C.-Y. Lin, S.-Y. Wang, D.-Y. Lee and T.-Y. Tseng, *J. Electrochem. Soc.*, 2008, **155**, H615.
11 F. Walz, *J. Phys.: Condens. Matter*, 2002, **14**, R285.
12 J. García and G. Subías, *J. Phys.: Condens. Matter*, 2004, **16**, R145.
13 M. Prades, N. Masó, H. Beltrán, E. Cordoncillo and A. R. West, *J. Mater. Chem.*, 2010, **20**, 5335–5344.
14 N. Masó and A. R. West, *Chem. Mater.*, 2012, **24**, 2127–2132.
15 Q.-L. Zhang, N. Masó, Y. Liu, H. Yang and A. R. West, *J. Mater. Chem.*, 2011, **21**, 12894–12900.
16 L. Gil Escrig, M. Prades, H. Beltrán, E. Cordoncillo, N. Masó and A. R. West, *J. Am. Ceram. Soc.*, 2014, **97**, 2815–2824.
17 M. Mogensen, N. M. Sammes and G. A. Tompsett, *Solid State Ionics*, 2000, **129**, 63–94.
18 Y. Xiong, K. Yamaji, N. Sakai, H. Kishimoto, T. Horita, M. E. Brito and H. Yokokawa, *J. Electrochem. Soc.*, 2006, **153**, A2198.
19 F. Yang, X. Zhao and P. Xiao, *J. Power Sources*, 2011, **196**, 4943–4949.
20 G. Varvoutis, M. Lykaki, G. E. Marnellos and M. Konsolakis, *Catalysts*, 2023, **13**, 275.
21 X. Guo, S. Mi and R. Waser, *Electrochem. Solid-State Lett.*, 2005, **8**, J1–J3.
22 S. Omar, E. D. Wachsman, J. L. Jones and J. C. Nino, *J. Am. Ceram. Soc.*, 2009, **92**, 2674–2681.
23 X. Guo, W. Sigle and J. Maier, *J. Am. Ceram. Soc.*, 2003, **86**, 77–87.
24 H. Tuller and A. Nowick, *J. Electrochem. Soc.*, 1979, **126**, 209.
25 N. Masó and A. R. West, *Chem. Mater.*, 2015, **27**, 1552–1558.
26 A. R. West, *J. Mater. Chem. A*, 2023, **11**, 12681–12694.
27 M. Jovaní, H. Beltrán-Mir, E. Cordoncillo and A. R. West, *Sci. Rep.*, 2019, **9**, 18538.
28 A. M. Rana, M. Ismail, E. Ahmed, I. Talib, T. Khan, M. Hussain and M. Nadeem, *Mater. Sci. Semicond. Process.*, 2015, **39**, 211–216.
29 C.-Y. Lin, D.-Y. Lee, S.-Y. Wang, C.-C. Lin and T.-Y. Tseng, *Surf. Coat. Technol.*, 2008, **203**, 480–483.
30 M. Ismail, A. Ahmad, K. Mahmood, T. Akbar, A. M. Rana, J. Lee and S. Kim, *Appl. Surf. Sci.*, 2019, **483**, 803–810.
31 H. Li, T. Liu, Y. Wang, S. Geng, T. Xu, M. Cao, S. Fan, T. Liu and J. Su, *Ceram. Int.*, 2022, **48**, 13754–13760.
32 W. Wang, B. Zhang and H. Zhao, *Results Phys.*, 2020, **16**, 103001.